Kinetics Studies of Solvent-Induced Crystallization of Drawn Poly(ethylene Terephthalate) by the In Situ Density Measurement

SUNG SOON IM and HYUNG SICK LEE, *Department of Textile Engineering, College of Engineering, Han Yang University, Seoul, Korea*

Synopsis

The effect of draw ratios on the solvent-induced crystallization (SINC) of poly(ethylene terephthalate) (PET) films was investigated. Dimethyl formamide (DMF) and dioxane were used as strongly interacting solvents. A newly devised *in situ* density measuring apparatus was applied to directly examine solvent penetration kinetics in PET. In this article, the density of PET films, which had a linear relation with crystallinity, was estimated rather than the degree of crystallinity. The solvent-penetrated PET film was divided into three regions: a surface-cavitated, a crystalline-swollen, and an unpenetrated region, to determine the specific characteristics of the respective regions. It was found that the density in the internal region and the fraction of the surface-cavitated region had a larger dependence on draw ratio than on treatment temperature. Also, the diffusion coefficients for the crystalline swollen region were calculated at various draw ratios and the morphological structure of the PET films was described.

INTRODUCTION

It is generally recognized that, in the presence of certain interactive solvents, crystallization of amorphous polymers can take place at temperatures well below the glass transition temperature (T_g) of the polymer. Previous studies associated with the solvent-induced crystallization (SINC) of poly(ethylene terephthalate) (PET) have focused on solvent–PET interaction, diffusion, crystallization kinetics, and morphology.

In the studies of solvent–PET interaction, the equilibrium density, volumetric swelling,[1,2] and equilibrium crystallinity based on infrared (IR) studies[3] were used. Ribnick et al.[3-6] working with fibers, correlated the lowering of the glass transition temperature to solubility parameter. They also suggested a bimodal distribution of mechanical properties as a function of total solubility parameter. The solubility parameters of solvents which have the most pronounced effect were 10.0 and 12.1.[7] On the other hand, Desai and Wilkes[8] reported that the characteristic morphology by SINC of PET was spherulitic and it was fast and fully developed just behind a diffusion front. They also observed a surface-cavitated texture using a scanning electron microscope (SEM). Makarewicz and co-workers[8-10] indirectly showed that the morphological nature of PET films in SINC involved a laminated-type structure composed of a swollen crystallized layer, an unpenetrated layer, and a surface-cavitated layer.

Journal of Applied Polymer Science, Vol. 37, 1801–1814 (1989)

CCC 0021-8995/89/071801-14$04.00

Weight uptake kinetics of various interactive solvents were investigated in the diffusion studies. The sorption behavior was apparently Fickian.[8,10] Makarewicz and Wilkes[11] calculated the spherulitic growth rates for SINC on the basis of the kinetic nucleation model and the classic theory of polymer diluent crystallization. Instead of the experimental measurements of glass transition (T_g) and transition melting (T_m) temperatures for polymer solvent system, they estimated T_g and T_m by the Flory equation and the Kelly-Beuche equation, respectively, and their result for the spherulitic growth rate seems to fit the SINC kinetics. A mathematical model for diffusion with the solvent-induced crystallization was proposed by Durning and Russel,[12,13] where crystallization and diffusion kinetics in the SINC process have been combined.

Concerning the effect of orientation and prior crystallization on the SINC of PET, Jameel et al.[14] reported that the overall diffusion behavior was found to be Fickian, and solvent diffusion and the extent of SINC decreased with increasing orientation and crystallinity in the starting films. In their subsequent report,[15] they found that an internal void structure was formed due to the crystallization taking place in a swollen state. Their results have indicated that the size of the void was nearly independent of treating temperatures while the contents of the void was increased with immersion temperature and draw ratio.

All of the above methods for investigating SINC phenomena were not *in situ* methods, specifically, procedure of the sample removal followed by blotting or drying was inevitably necessary. Thus, in this report, the *in situ* density measurement was introduced by using a newly designed apparatus which directly measured immersion weight during the SINC process. Furthermore, crystallization and diffusion kinetics were investigated at various draw ratios of PET films by using the *in situ* density measurement.

EXPERIMENTAL

Material

Initially amorphous, unoriented PET films were obtained through the courtesy of the Sun Kyung Chemical Company. The PET films were uniaxially drawn at 80–90°C using two pair of rollers, rotating at different speeds, which determined the draw ratio. A range of draw ratios between 1.0 and 4.0 was provided and the thickness and density of the samples corresponding to the various draw ratios are shown in Table I. Dimethyl formamide (DMF) and dioxane were used as a strong interactive solvent with PET.

Method and Apparatus

For the *in situ* measurement of density during SINC, the apparatus shown in Figure 1 was devised. A bath was installed with control switch, transformer, immersion heater, and thermosensor for keeping constant temperature. The apparatus was equipped with a balance. After filling the bath with solvent and immersing the sample, the density of sample during SINC could be directly determined, that is, the density of the immersed sample was calculated from the change in the bouyant force. The weight of the sample

TABLE I
PET Film Properties

Draw ratio	Thickness (μm)	Density[a]
1.0	250	1.3368
2.0	177	1.3374
2.5	158	1.3381
3.0	144	1.3480
3.5	134	1.3528

[a]Using density gradient column at 23°C.

immersed in solvent, m_b is given by the following equations:

$$m_b = m - v\rho_s + m_w - \pi r^2 l\rho_w \tag{1}$$

$$m_b = m - m\rho_{s/\rho} + m_w - \pi r^2 l\rho_w \tag{2}$$

where, m and m_w are the weight of starting film, and the weight of wire, respectively; ρ, ρ_s, and ρ_w are the density of the immersed sample, solvent, and wire, respectively; π is the circular constant, v is the volume of the immersed sample; and, r, l are the radius and length of the immersed wire, respectively.

When $\rho(t)$ and $m_b(t)$ represent ρ and m_b as functions of time, the density of sample, $\rho(t)$, at any time during SINC is given by:

$$\rho(t) = \frac{m\rho_s}{m + m_w - \pi r^2 l\rho_w - m_b(t)} \tag{3}$$

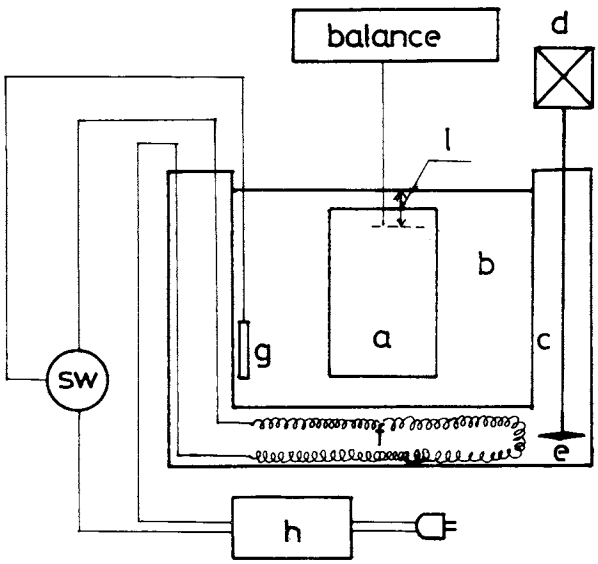

Fig. 1. Schematic diagram of density measuring apparatus.

To evaluate the density at the equilibrium state, solvent removal was performed by immersing the swollen samples for three days at room temperature in methanol, which is compatible with DMF and dioxane but cannot induce crystallization of PET. The samples were subsequently dried for 3 days in vacuo. The density of the dried films was determined by density gradient column at 23°C.

RESULTS AND DISCUSSION

During solvent sorption, solvent molecules migrate toward the center line of the PET film. Since the strong interaction between the PET and solvents is responsible for the inducement of the plasticization or increased mobility in amorphous regions of the PET. Crystallites then develop and grow to their maximum size. Clearly, the overall crystallization is governed by two rate processes: solvent migration into the sample and crystallite growth in the plasticized elements of the samples. The slower process will control the overall crystallization rate. Figures 2–5 show density data for the oriented PET films of selected draw ratios at various DMF and dioxane treatment temperatures. The density data were plotted as a function of time$^{1/2}/d$ (d is the half of the film thickness) for data comparison, since the thickness of the samples varies with draw ratio. The initial portion of the density curves was always linear with the square root of the immersed time. It indicates that these are diffusion-controlled systems.

It is interesting that, when the initial linear portion of the density curves is extrapolated to zero time, the density value at zero time is not the same as the density of the starting films shown in Table I. These different density values can be explained as follows; before the beginning of solvent migration, the polymer molecules on the film surface contact with the solvent which induces very rapid crystallization. Thus, in this region the density is increasing at a very rapid rate which cannot be measured *in situ*. It can be seen that extrapolated zero-time densities of the samples with low draw ratio are larger values than shown in Table I. The fact that the extrapolated zero-time densities of low draw ratio samples were greater than those of high draw ratio samples can be explained by the extent of surface-cavitated regions, that is, it could be considered that high draw ratio samples have a smaller extent of surface crystallization.

Figure 6 shows the schematic structure of a partially swollen film as an ideal laminated model. This structure had been verified by Makarewicz et al.[9] Such an ideal laminated model should have a density value, $\rho(t)$, as a function of time given by:

$$\rho(t) = \rho_u(1 - f_s - f_c) + \rho_s f_s + \rho_c f_c \tag{4}$$

where,

$$f_c = \frac{w_c}{w_c + w_s + w_u} \tag{5a}$$

$$f_s = \frac{w_s}{w_c + w_s + w_u} \tag{5b}$$

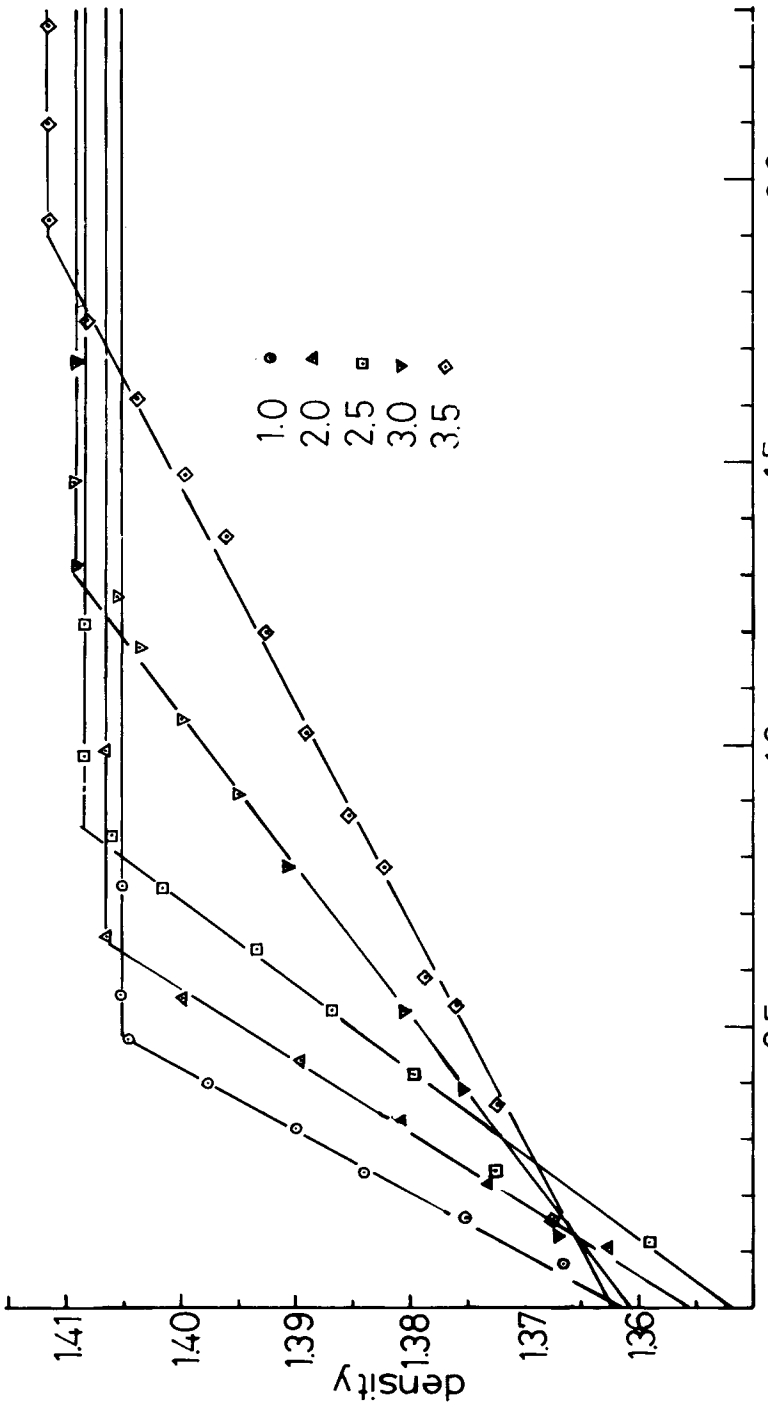

Fig. 2. Density vs. $\sqrt{t}/d$ for DMF (23°C) treated films of various draw ratios (⊙) 1.0, (▲) 2.0, (⊡) 2.5, (▼) 3.0, (◇) 3.5.

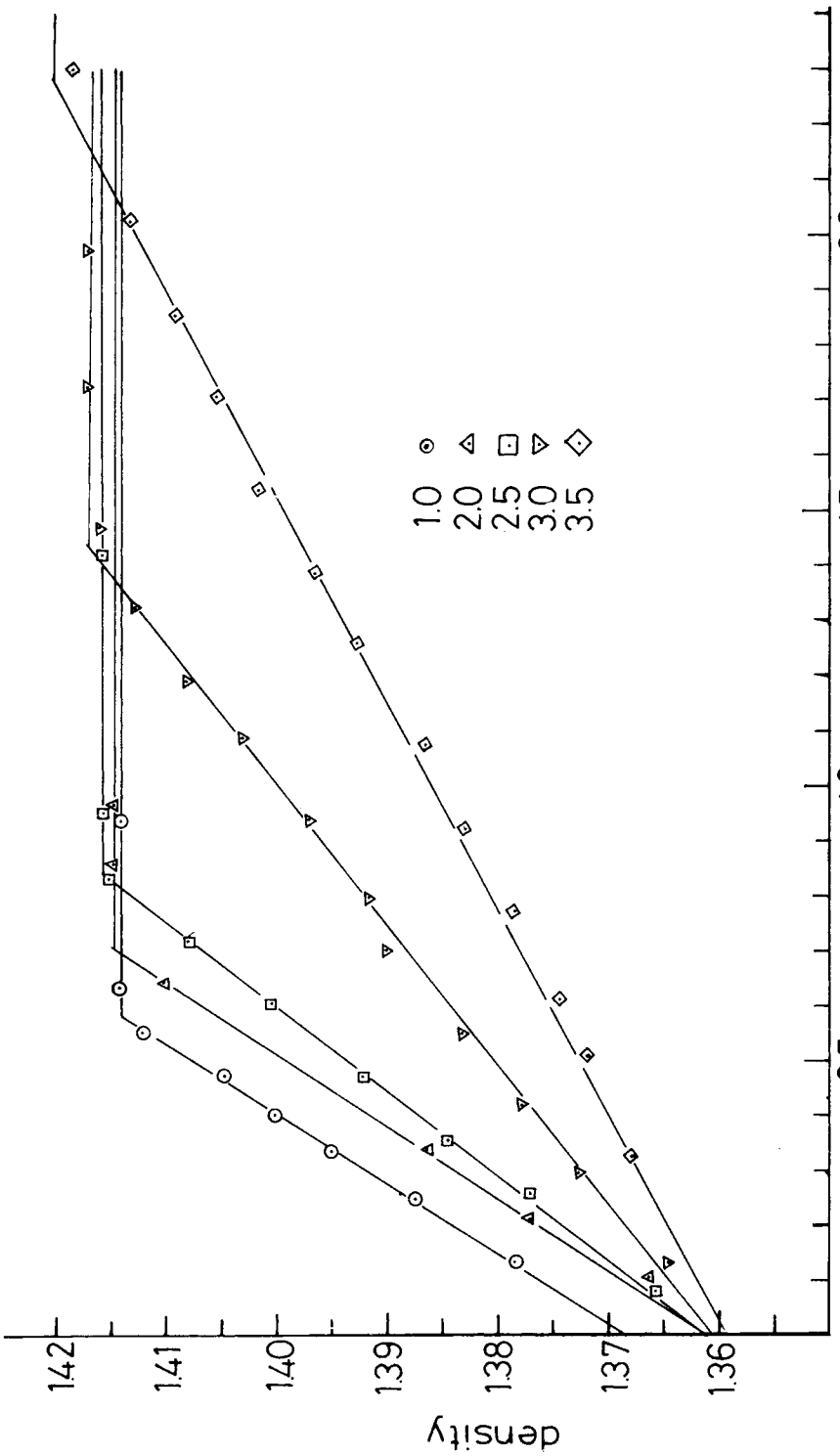

Fig. 3. Density vs $\sqrt{t}/d$ for dioxane (23°C) treated films of various draw ratios (⊙) 1.0, (▲) 2.0, (⊡) 2.5, (▼) 3.0, (◇) 3.5.

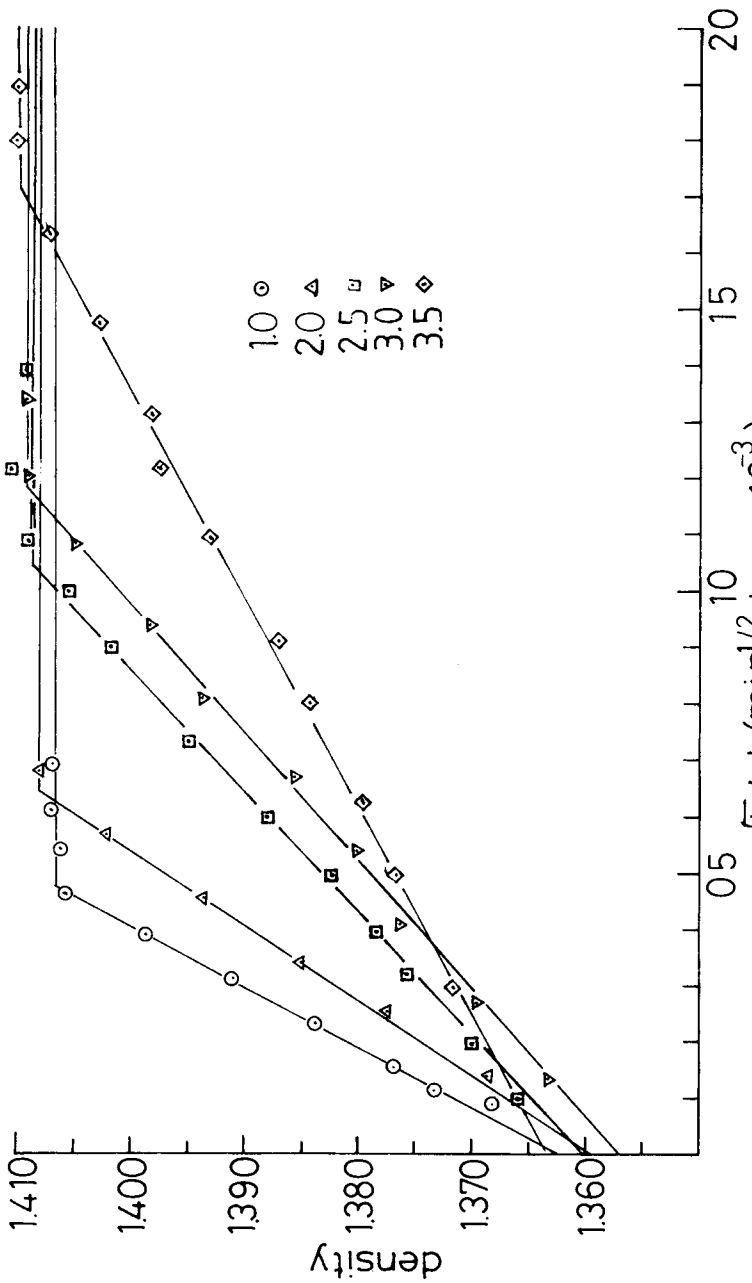

Fig. 4. Density vs. $\sqrt{t}/d$ for DMF (30°C) treated films of various draw ratios (⊙) 1.0, (▲) 2.0, (⊡) 2.5, (▼) 3.0, (◇) 3.5.

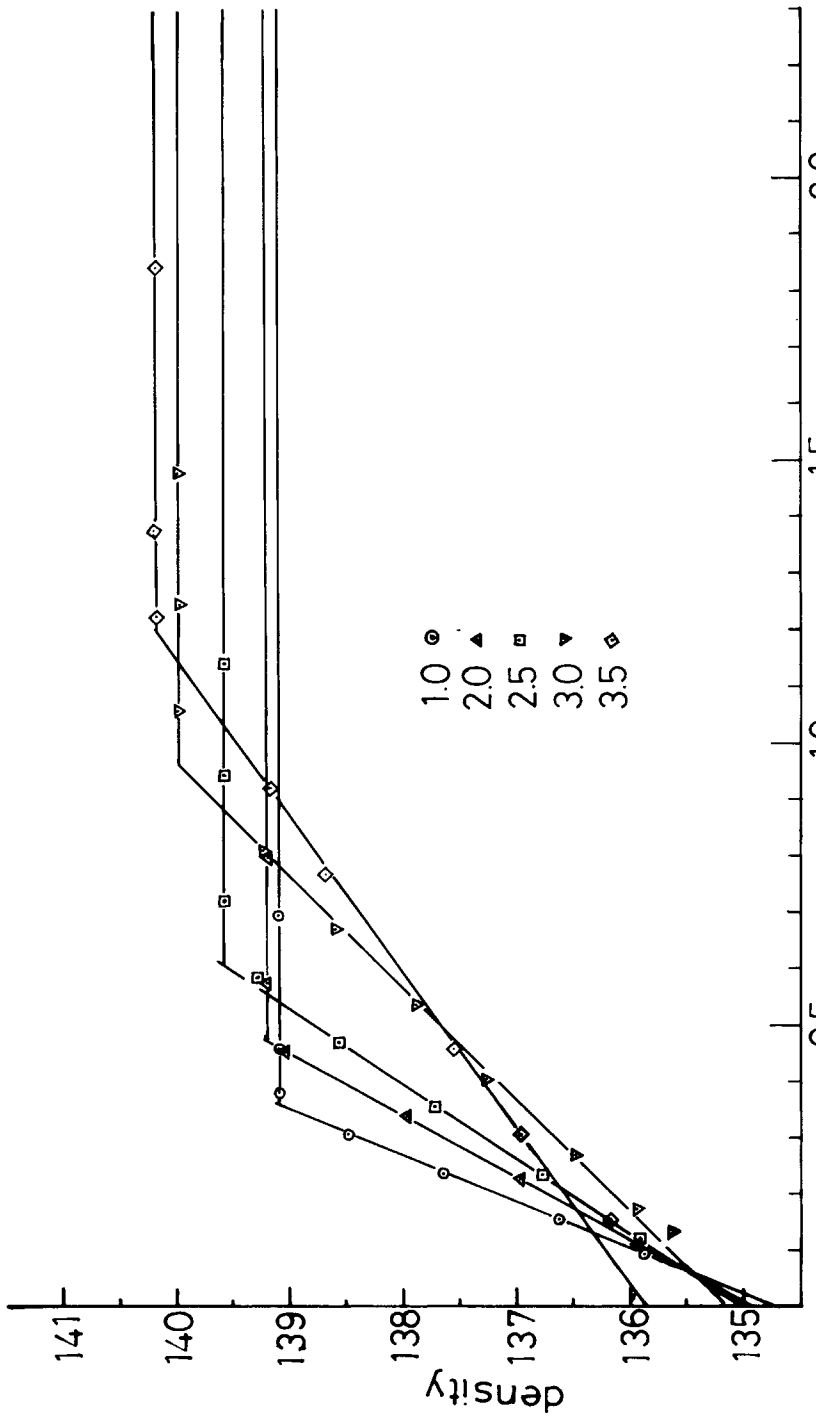

Fig. 5. Density vs. $\sqrt{t}/d$ for DMF (50°C) treated films of various draw ratios (⊙) 1.0, (▲) 2.0, (⊡) 2.5, (▼) 3.0, (◇) 3.5.

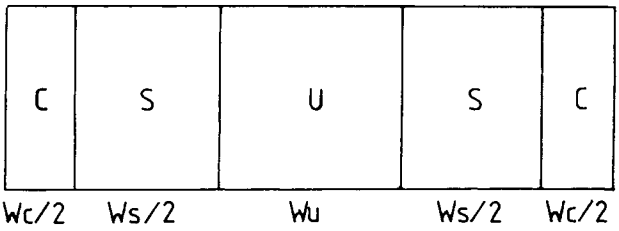

Fig. 6. Schematic diagram of an ideal laminate model.

are the effective thickness fractions, which are equal to volume fraction, of the three elements in the model. The subscripts c, s, and u refer to the surface-cavitated, the swollen crystallized, and unpenetrated layers, respectively. W is the thickness of the layer and ρ_c, ρ_s, and ρ_u correspond to the density values of the respective layers.

The density values at zero time, which is the extrapolated zero-time density, is expressed by the following equation:

$$\rho(0) = \rho_u(1 - f_c) + \rho_c f_c \tag{6}$$

The density of the surface-cavitated layer, ρ_c, which shows that the SINC process accomplished a nearly perfect crystal on the film surface, was estimated to be 1.4555 g/cm^3 by the density gradient column at 23°C. The density values of the unpenetrated layer, ρ_u, were replaced by those of the starting films shown in Table I, and the density values of the film at zero time, $\rho(0)$, were calculated with the thermal volume expansion coefficient of PET at 23°C (3.94×10^{-4}/°C).[16]

In Table II, $\rho(0)$ and $\rho(\infty)$ represent density values at zero time and the equilibrium state, and $\rho^*(0)$ and $\rho^*(\infty)$ are corrected to 23°C by using the thermal volume expansion coefficient of PET. By using the density values of ρ_u, ρ_c, and $\rho(0)$, the volume fraction of the surface cavitation, f_c, has been calculated and is shown in Table III.

The quantity of the surface cavitation generally decreased with increasing orientation and crystallinity in the starting films but changed little with the treating temperature. We believe that, in high draw ratio samples, the surface

TABLE II
Initial and Equilibrium Densities of Solvent Treatment at Each Temperature

Draw ratio	23°C				30°C				50°C			
	DMF		Dioxane		DMF				DMF			
	$\rho(0)$	$\rho(\infty)$	$\rho(0)$	$\rho(\infty)$	$\rho(0)$	$\rho(\infty)$	$\rho(0)^*$	$\rho(\infty)^*$	$\rho(0)$	$\rho(\infty)$	$\rho(0)^*$	$\rho(\infty)^*$
1.0	13609	1.4053	1.3686	1.4140	1.3607	1.4055	1.3645	1.4094	1.3493	1.3912	1.3638	1.4062
2.0	1.3546	1.4064	1.3603	1.4142	1.3594	1.4075	1.3632	1.4114	1.3497	1.3923	1.3642	1.4073
2.5	1.3511	1.4082	1.3602	1.4152	1.3596	1.4081	1.3633	1.4124	1.3507	1.3971	1.3652	1.4121
3.0	1.3611	1.4092	1.3602	1.4172	1.3582	1.4086	1.3620	1.4125	1.3515	1.4014	1.3660	1.4165
3.5	1.3643	1.4117	1.3617	1.4207	1.3633	1.4097	1.3671	1.4136	1.3591	1.4021	1.3737	1.4172

*Densities rendered at 23°C by calculating with the thermal expansion coefficient of PET (ref. 18).

TABLE III
Fractions of the Cavitated Regions and Densities of the Swollen Crystallized Regions[a]

Draw ratio	23°C				30°C		50°C	
	DMF		Dioxane		DMF		DMF	
	f_c	ρ_s	f_c	ρ_s	f_c	ρ_s	f_c	ρ_s
1.0	0.204	1.3926	0.269	1.3989	0.234	1.3955	0.228	1.3918
2.0	0.146	1.3980	0.195	1.4043	0.219	1.3992	0.228	1.3932
2.5	0.111	1.4023	0.189	1.4059	0.216	1.4006	0.232	1.3991
3.0	0.122	1.4028	0.114	1.4123	0.130	1.4061	0.202	1.4068
3.5	0.113	1.4062	0.087	1.4174	0.140	1.4063	0.205	1.4075

[a] Data were calculated using the $\rho(0)^*$ and $\rho(\infty)^*$ of Table II.

craze causes the f_c values to be greater than in low-draw ratio samples. Obviously, it was recognized that the extent of the surface cavitation was influenced by the surface craze; this was also reported by Desai and Wilkes.[8] The drawing method in our experiments imposed a surface-crazed layer with the higher draw ratio samples. At higher treating temperature, it was found that the extent of the surface cavitation decreased little with increasing draw ratio. In addition, it was observed that dioxane solvent had a stronger ability to induce surface cavitation than DMF.

When the penetration is completed, Eq. (4) can be modified by using $f_s = 1 - f_c$;

$$\rho(\infty) = \rho_s(1 - f_c) + f_c\rho_c \tag{7}$$

In order to calculate the density of the swollen region, ρ_s, the values of $\rho(\infty)^*$ evaluated by thermal volume expansion coefficient of PET were substituted for $\rho(\infty)$ and the f_c values shown in Table III were used in Eq. (7).

The density difference $(\rho_s - \rho_u)$ is proportional to the extent of SINC excluding the surface-cavitated region and shown in Table IV. It was found that the fraction of swollen crystalline region was a maximum value at draw ratio 2.5. Jameel et al.[15] found that the size of the spherulite has a maximum value at draw ratio 2.8. Three results suggested that SINC did not nucleate new crystallites, but promoted the existing crystallite's growth.

TABLE IV
Increased Density by SINC in the Swollen Crystallized Region[a]

Draw ratio	23°C				30°C		50°C	
	DMF		Dioxane		DMF		DMF	
	$\rho_s - \rho_u$	$X_s - X_u$	$\rho_s - \rho_u$	$X_s - X_u$	$\rho_s - \rho_u$	$X_s - X_u$	$\rho_s - \rho_u$	$X_s - X_u$
1.0	0.0588	46.5	0.0621	51.8	0.0587	48.9	0.0550	45.8
2.0	0.0606	50.5	0.0669	55.8	0.0618	51.5	0.0558	46.5
2.5	0.0642	53.5	0.0678	56.5	0.0623	51.9	0.0610	50.8
3.0	0.0548	45.7	0.0643	53.6	0.0581	48.5	0.0588	49.0
3.5	0.0534	44.5	0.0646	53.8	0.0541	45.1	0.0547	45.6

[a] X_s and X_u were degrees of crystallinity, in which suffix, S and U were identified as Fig. 6.

The straight lines in Figures 2–5 mean that, since the rate of the crystallization is much faster than that of the penetration, the penetration rates can be determined from the data. The initial stages of the density curve shown in Figures 2–5 would not be linear if the crystallization rates were not fast. Accordingly, Figures 2–5 indicate Fickian penetration. Thus, the penetration distance is given by:

$$X = (Dt)^{1/2} \tag{8}$$

where, X is a penetration distance, D is a diffusion coefficient, and t is immersion time. When it is divided by total diffusion distance, $d' = d(1 - f_c)$, the fraction of crystalline and swollen region, f_s, is as follows:

$$f_s = \frac{X}{d'} = (Dt)^{1/2}/d' \tag{9}$$

Using Eq. (9), Eq. (4) can be modified:

$$\rho(t) = \rho_u + \rho_c f_c - \rho_u f_c + (Dt)^{1/2}(\rho_s - \rho_u)/d' \tag{10}$$

In order to evaluate the diffusion coefficient at various draw ratios, the horizontal axes of the density curves in Figures 2–5 were rescaled with total diffusion distance, d', and the density values shown in Table II were corrected to 23°C for data comparison. From these corrected data, the diffusion coefficients were calculated in Eq. (10) and shown in Table V. As expected, the diffusion rates were decreased with increasing draw ratio and increased with rising temperature. The crystallinity in dioxane–PET system was larger than in the DMF–PET system, it was found that the diffusion rate of dioxane was slower. This could indicate that, in dioxane–PET systems, the blocking factor would be enhanced by SINC.

Figure 7 shows SEM micrographs of the surface structure with different solvent systems. It appears that dioxane created a more severe cavitation than DMF and the lower draw ratio samples shows a more severe effect. Figure 8 shows micrographs of the scrapped surface structures, where the arrows indicate surface directions. It can be seen that the morphological structure in the internal region was quite different from the surface region. That is, the surface region formed a more severe cavitation than internal region.

TABLE V
Diffusion Coefficient at the Various Temperatures in Each Solvent (cm^2/s)

Draw ratio	23°C		30°C	50°C
	DMF	Dioxane	DMF	DMF
1.0	2.83×10^{-8}	1.63×10^{-8}	2.87×10^{-8}	1.03×10^{-7}
2.0	1.62×10^{-8}	1.51×10^{-8}	1.72×10^{-8}	6.02×10^{-8}
2.5	1.45×10^{-8}	9.92×10^{-9}	1.51×10^{-8}	3.02×10^{-8}
3.0	5.84×10^{-9}	5.11×10^{-9}	1.49×10^{-8}	1.39×10^{-8}
3.5	4.15×10^{-9}	2.32×10^{-9}	6.74×10^{-9}	1.05×10^{-8}

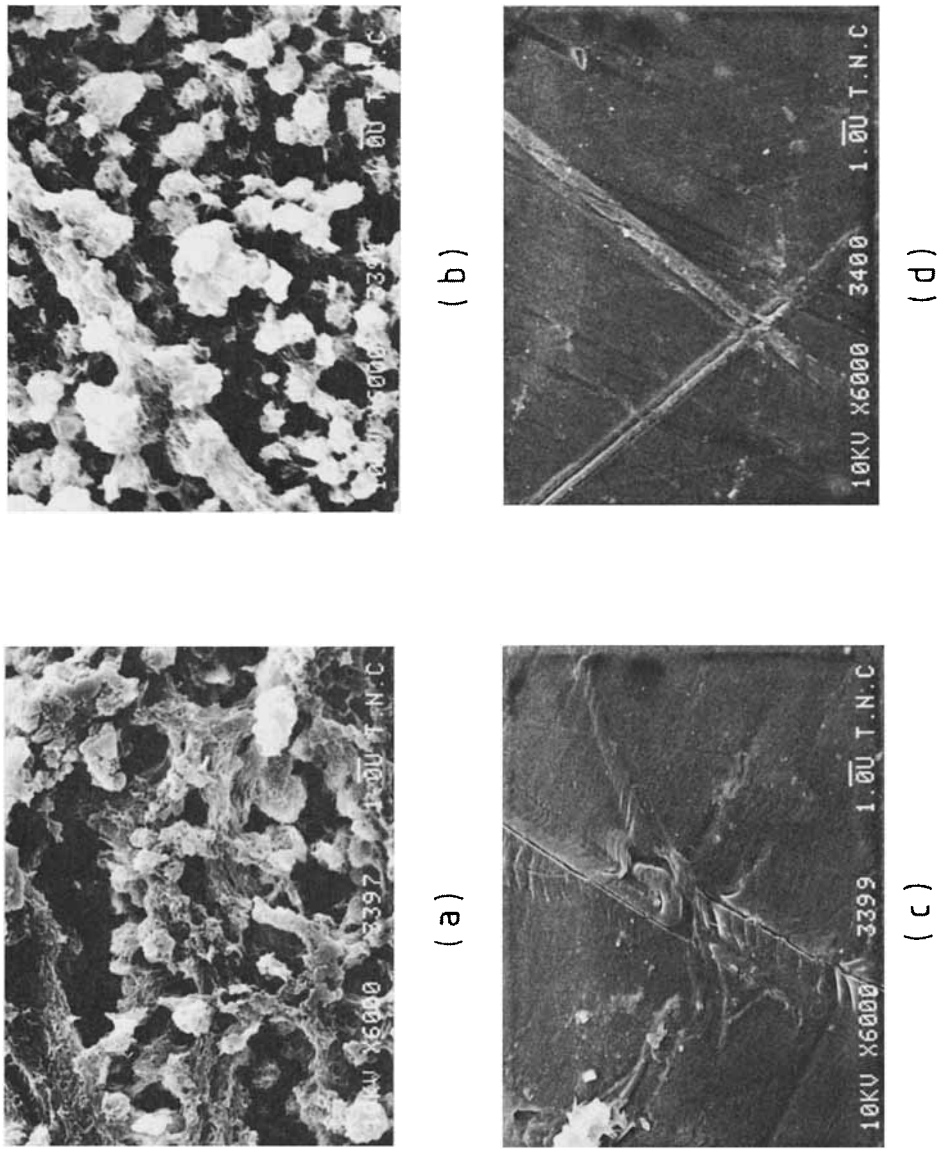

Fig. 7. Typical SEM micrographs of the surface.

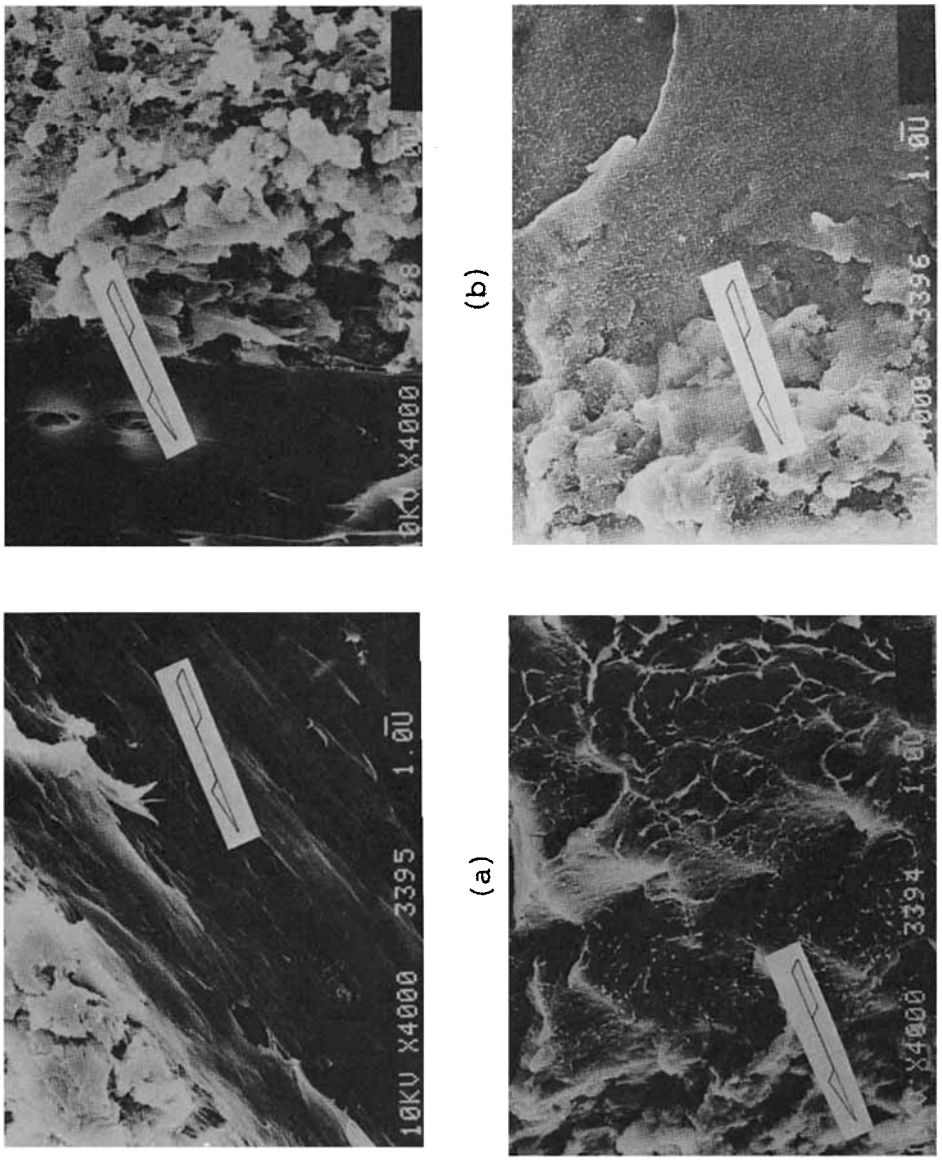

Fig. 8. Typical SEM micrographs of the scrapped and fractured surface.

CONCLUSION

The effect of draw ratios on the solvent-induced crystallization (SINC) of PET with two different solvent systems was investigated by a newly devised *in situ* density measuring apparatus. In the DMF- and dioxane-PET systems, SINC was diffusion controlled. In addition, the following facts were found: nearly perfect crystals were produced in the surface-cavitated region; a new nucleation does not seem to take place in the internal region; the extent of the surface-cavitated region decreased with increasing initial draw ratio and increased with elevating temperature. Finally, the diffusion rate in the internal region generally decreased with increasing draw ratio and increased with rising temperature.

The authors acknowledge support of this work by Academic Research Grant from the Korea Ministry of Education.

References

1. W. R. Moore and R. P. Sheldon, *Polymer*, **2**, 315 (1961).
2. R. P. Sheldon, *Polymer*, **3**, 27 (1962).
3. E. L. Lawton and D. M. Cates, *J. Appl. Polym.*, **13**, 897 (1969).
4. A. S. Ribnick, H. D. Weigmann, and L. Rebenfeld, *Textile Res. J.*, **43**, 123 (1973).
5. A. S. Ribnick and H. D. Weigmann, *Textile Res. J.*, **43**, 316 (1973).
6. A. S. Ribnick and H. D. Weigmann, *Textile Res. J.*, **44**, 165 (1974).
7. B. H. Knox, H. D. Weigmann, and M. G. Scott, *Textile Res. J.*, **45**, 203 (1975).
8. A. B. Desai and G. L. Wilkes, *J. Polym. Sci. Polym. Symp.*, **46**, 291 (1974).
9. P. J. Makarewicz, G. L. Wilkes, and Y. Budnitsky, *J. Polym. Sci., Polym. Phys. Ed.*, **16**, 1545 (1978).
10. P. J. Makarewicz and G. L. Wilkes, *J. Polym. Sci., Polym. Phys. Ed.*, **16**, 1529 (1978).
11. P. J. Makarewicz and G. L. Wilkes, *J. Polym. Sci., Polym. Phys. Ed.*, **16**, 1559 (1978).
12. C. J. Durning and W. B. Russel, *Polymer*, **26**, 119 (1985).
13. C. J. Durning and W. B. Russel, *Polymer*, **26**, 131 (1985).
14. H. Jameel, J. Waldman, and R. Ludwig, *J. Appl. Poly. Sci.*, **26**, 1795 (1981).
15. H. Jameel, D. N. Herman, and R. Ludwig, *J. Appl. Polym. Sci.*, **27**, 773 (1982).
16. H. J. Kolb and E. F. Izard, *J. Appl. Phys.*, **20**, 564 (1949).

Received July 22, 1987
Accepted January 15, 1988